Algebraic filters for filtered backprojection

Plantagie, L.

1

INTRODUCTION

1.1 X-RAY TRANSMISSION COMPUTED TOMOGRAPHY

Computed tomography is a technique that is used to reconstruct an object from a set of projections. It is applied in a broad range of fields, for example electron tomography, (bio)medical imaging, industrial imaging (such as quality inspection for materials science), and seismic tomography. The resolution depends upon the object to be scanned and can vary from nanometers to kilometers [1–5].

For X-ray transmission computed tomography, the projections are obtained by sending X-ray beams under varying angles through the object and measuring the intensity profile of the X-ray beam at a detector after it has traversed the object. The difference in intensity of the beam before and after intersecting the object, i.e. the *attenuation*, is used as input for various algorithms that can compute an image of the interior of the object. The attenuation of the beam is related to the type and thickness of the materials that lie on the ray paths between the X-ray source and the detector, and also on the energy of the X-ray photons that are used. This will be made more precise in the following.

We now consider a two-dimensional object, i.e. a slice. Let $\mu(x, y, E)$ denote the attenuation coefficient of the material at position $(x, y) \in \mathbb{R}^2$ for energy level E. Let L be a line from the source to the detector that is parameterized by $L(l)$, i.e., the variable l denotes the position on the line L. Let $I_{in}(E)$ denote the intensity of the beam at energy E before it intersects with the object. The total intensity I of the beam at position l_1 is then given by Eq. (1.1) [6].

$$I(l_1) = \int_0^{E_{max}} I_{in}(E) e^{-\int_0^{l_1} \mu(L(l),E)\,dl}\,dE, \tag{1.1}$$

where $I_{in}(E)$ is the intensity of the incident beam.

In this work we mainly focus on monochromatic X-ray beams, i.e. beams with only one energy level E_0. In this case, there is a single attenuation for each position (x, y) in the object, which we denote by $f(x, y) = \mu(x, y, E_0)$. Then Eq. (1.1) simplifies to Eq. (1.2), which is known as the *Lambert-Beer* law [6, 7].

$$I(l_1) = I_{in} e^{-\int_0^{l_1} f(L(l))dl}. \tag{1.2}$$

Let I_{out} be the intensity of the beam after traversing the object. We then define the *projection* of the object along the line L by Eq. (1.3).

$$p_L = -\ln\left(\frac{I_{out}}{I_{in}}\right) = \int_L f(L(l))dl, \tag{1.3}$$

where ln denotes the natural logarithm.

We conclude that by recording the intensities of both the attenuated beam and the unattenuated beam (without an object in the scanner), the integral of the attenuation along lines through the object can be obtained.

For a line L given in Eq. (1.4), the line integral along L is given by Eq. (1.5). This transform has been introduced by Johann Radon in 1917 [8] and is now known as the Radon transform [6, 9, 10].

$$L \ : \ x\cos\theta + y\sin\theta = t, \ \text{for some } t \in \mathbb{R}, \tag{1.4}$$

$$(\mathcal{R}f)(\theta, t) = \int_{-\infty}^{\infty} f(t\cos\theta - s\sin\theta, t\sin\theta + s\cos\theta)\, ds, \tag{1.5}$$

for $t \in \mathbb{R}$ and $\theta \in [0, 2\pi)$.

The Radon transform is of great importance in Computed Tomography. In 2D parallel beam scanning techniques, a detector is located opposite an X-ray source. In this work, we assume the detector is situated along a straight line perpendicular to a parallel beam of X-ray as shown in Fig. 1.1a. This figure also illustrates the concept of the line integrals for the Shepp-Logan phantom. The Shepp-Logan phantom is an image that consists of ellipses with different gray levels. It resembles a cross-section of a human head.

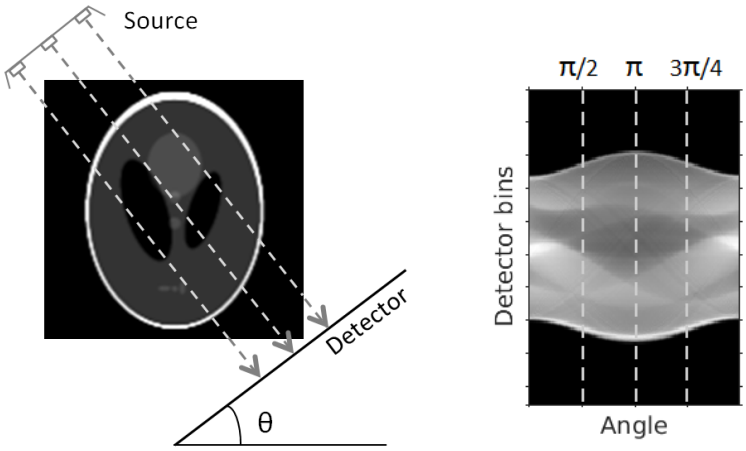

(a) Object space (b) Radon space

Figure 1.1: (a) 2D Parallel beam scanning geometry, (b) Projection data in Radon space.

The measured projection data can now be written as a set of line integrals depending on the projection angle $\theta \in [0, \pi)$ and position t on the detector (see Eq. (1.6)).

$$p(\theta, t) = (\mathcal{R}f)(\theta, t). \tag{1.6}$$

The projection data for the phantom in Fig. 1.1a is shown in Fig. 1.1b. The gray level corresponds to the attenuation, where black refers to no attenuation and white to high attenuation.

There exist exact inversion formulas for the Radon Transform, such as the inverse Radon Transform [8] and the Fourier Slice theorem [6, 7, 9, 11]. However, these inversion formulas are based on the assumption that projections are available for all angles θ and for all detector coordinates t. Since in practice only a finite set of projection angles Θ can be measured for a finite set of detector bins T, such inversion formulas cannot be used directly as a reconstruction algorithm. Therefore, reconstruction methods have been developed that *approximate* the object. These methods can roughly be divided into two categories: *analytical* reconstruction methods and *algebraic* reconstruction methods (ARMs). A well-known reconstruction method in the analytical group is *Filtered*

1

Backprojection (FBP). We will now consider both FBP and the algebraic reconstruction methods in more detail.

1.2 FBP

An intuitive way to approximate the unknown function f is to take each element of the projection data and backproject it along its corresponding line through the object. Pixels that are contained in the support of the function f receive positive contributions from the corresponding backprojected lines for all projection angles. Pixels outside f receive in general only contributions for a smaller set of projection angles and their value in the reconstruction is less than that of pixels inside f. As attenuation coefficients are always positive values, the reconstruction of this backprojection method is a nonnegative image.

A major drawback of this method is that the reconstructed image is blurred and does not correctly invert the Radon transform. The Fourier Slice Theorem provides a more accurate inversion formula, which combines the backprojection operation with a *filtering* step [6, 7, 9, 11]. Let $P(\theta,\nu) = \int_{-\infty}^{\infty} p(\theta,t)e^{-2\pi i\nu t}dt$, the one-dimensional Fourier transform of p, taken separately for each angle θ. According to the Fourier Slice Theorem, we can calculate f from P as shown in Eq. (1.7).

$$f(x,y) = \int_0^{\pi}\int_{-\infty}^{\infty} P(\theta,\nu)|\nu|e^{i2\pi\nu t}d\nu d\theta, \tag{1.7}$$

$$= \int_0^{\pi} q(\theta,t)d\theta, \tag{1.8}$$

where $t = x\cos\theta + y\sin\theta$ and $q(\theta,t) = \int_{-\infty}^{\infty} P(\theta,\nu)|\nu|e^{i2\pi\nu t}d\nu$.

The term $|\nu|$ is the important difference between the backprojection method described above and the formula in Eq. (1.7). The formula in Eq. (1.8) is a backprojection of the *filtered* projection data q, which is obtained by applying the so-called ramp-filter to the original projection data p. Note that for $G(\theta,\nu) = |\nu|$ the function q is defined as $q(\theta,t) = \int_{-\infty}^{\infty} P(\theta,\nu)G(\theta,\nu)e^{i2\pi\nu t}d\nu$. If we denote the inverse Fourier transform of $G(\theta,\cdot)$ by $g(\theta,\cdot)$, then Eq. (1.9) follows from the properties of the Fourier transform.

$$q(\theta,t) = \int_{-\infty}^{\infty} p(\theta,\tau)g(\theta,t-\tau)d\tau. \tag{1.9}$$

Hence $q(\theta, \cdot)$ equals the convolution of $p(\theta, \cdot)$ with the *filter* $g(\theta, \cdot)$.

Combining Eq. (1.8) and Eq. (1.9) and discretizing this formula results in Eq. (1.10), where $\mathbf{u}(x, y)$ denotes the value of the reconstructed image at coordinate (x, y). This formula is known as Filtered Backprojection.

$$\mathbf{u}(x, y) = \sum_{\theta \in \Theta} \sum_{t \in T} p(\theta, \tau) \tilde{g}(\theta, t - x\cos\theta - y\sin\theta), \tag{1.10}$$

where $\tilde{g}(\theta, t) = \frac{\pi}{|\Theta|} g(\theta, t)$.

Due to the limited number of projection data that can be measured, FBP can only compute an approximation of the unknown object f. The reconstruction quality of this approximation highly depends on the choice for the filter g. In 1971, Ramachandran and Lakshminarayanan have proposed to use a windowed filter for FBP [12]. We will refer to it as the Ram-Lak filter Eq. (1.11).

$$(\mathrm{Ram-Lak}) \qquad G(\theta, \nu) = |\nu| \operatorname{rect}(\nu), \tag{1.11}$$

where $\operatorname{rect}(\nu)$ equals 1 for $\nu \in [-\epsilon, \epsilon]$ for some $\epsilon > 0$ and 0 otherwise. This windowed function reduces the effects of noise in the high frequency domain, which would otherwise be amplified due to the multiplication with $|\nu|$. To further reduce the effects of amplifying the high frequencies, other windowed filters have been proposed in literature. For example the Shepp-Logan filter, Hann filter, Cosine filter, and Hamming filter, see Eq. (1.12)-Eq. (1.15) respectively [6].

$$(\mathrm{Shepp-Logan}) \quad G(\theta, \nu) = |\nu| \operatorname{rect}(\nu) \operatorname{sinc}(\nu), \tag{1.12}$$

$$(\mathrm{Hann}) \quad G(\theta, \nu) = |\nu| \operatorname{rect}(\nu)(0.5 - 0.5\cos(2\pi\nu)), \tag{1.13}$$

$$(\mathrm{Cosine}) \quad G(\theta, \nu) = |\nu| \operatorname{rect}(\nu) \cos(\pi\nu), \tag{1.14}$$

$$(\mathrm{Hamming}) \quad G(\theta, \nu) = |\nu| \operatorname{rect}(\nu)(0.54 - 0.46\cos(2\pi\nu)), \tag{1.15}$$

The main advantage of the Filtered Backprojection is its computational efficiency. It is also easy to implement and known for its high accuracy for low-noise projection data with a substantial number of equiangularly distributed projection angles. The reconstruction accuracy degrades in case of a limited angular range, few projection angles or a low signal-to-noise ratio. Fig. 1.2 contains reconstructions of

(a) Shepp-Logan phantom

(b) FBP

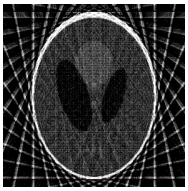

(c) FBP, $|\Theta| = 16$

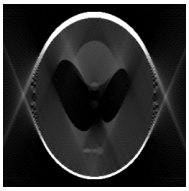

(d) FBP, AR $= 135°$

(e) FBP, $I_0 = 10^4$

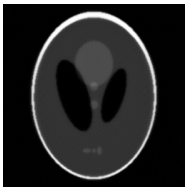

(f) SIRT

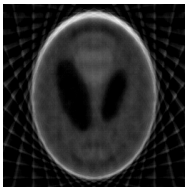

(g) SIRT, $|\Theta| = 16$

(h) SIRT, AR $= 135°$

(i) SIRT, $I_0 = 10^4$

Figure 1.2: Reconstructions for SIRT with 100 iterations and FBP with the Ram-Lak filter; unless stated differently, the parameters are $n = 255$, $|\Theta| = 128$, angular range (AR) $= 180°$ and noiseless projections.

the well-known Shepp-Logan phantom of both FBP and the algebraic reconstruction method SIRT (which will be discussed in Section 1.3) for varying parameters. The Shepp-Logan phantom consists of $n \times n$ pixels. The variable I_0 indicates the noise level. It represents the number of counts per detector element without an object.

1.3 ALGEBRAIC RECONSTRUCTION METHODS

Algebraic reconstruction methods offer an alternative approach to solving the reconstruction problem. Since the tomographic reconstruction problem can often not be solved exactly, the reconstruction problem

is discretized such that we obtain a system of linear equations. The unknown object is represented on a grid, which we here assume to be a square, consisting of $n \times n$ pixels. The object is characterized by the vector $\mathbf{x} \in \mathbb{R}^{n^2}$, such that x_i corresponds to the density of the object on pixel $i \in \{1, 2, \ldots, n^2\}$. The contribution of every image pixel to a line integral is given by the *projection matrix* $\boldsymbol{W}$. The number of rows of $\boldsymbol{W}$ equals the number of projection angles $|\Theta|$ multiplied by the number of detector bins $|T|$. Hence the discrete reconstruction problem can be written as Eq. (1.16).

$$\boldsymbol{W}\mathbf{x} = \mathbf{p}, \tag{1.16}$$

where $\mathbf{p} \in \mathbb{R}^{N_{T\Theta}}$ is the projection data and $N_{T\Theta} = |T||\Theta|$.

The number of unknowns in this discrete reconstruction problem is typically very large and a solution cannot be calculated in reasonable time by explicit matrix inversion. Therefore, iterative algorithms have been proposed that solve for a least squares solution. Examples of such methods are ART/Kaczmarz method, SIRT and CGLS. We will now discuss SIRT in more detail.

The *Simultaneous Iterative Reconstruction Method* (SIRT) is an iterative linear reconstruction method. It updates the current solution based on the difference between the current forward projection and the measured projection data for all projection angles simultaneously. The kth iteration step of SIRT can be written as Eq. (1.17) [13, 14]. SIRT converges to a weighted least squares solution of the reconstruction problem.

$$\mathbf{u}^{(k+1)} = \mathbf{u}^{(k)} + \omega \boldsymbol{W}^T(\mathbf{p} - \boldsymbol{W}\mathbf{u}^{(k)}), \tag{1.17}$$

where $u^{(k)} \in \mathbb{R}^{n^2}$ is the resulting image of the k-th iteration and $\omega \in \mathbb{R}$ is a relaxation parameter.

A disadvantage of many algebraic reconstruction methods including SIRT is that they require a long computation time. By parallelizing the computations of SIRT and using GPUs, the reconstruction time can be substantially reduced [15–17]. However, for large reconstruction problems the reconstruction time required for SIRT is still much larger than for FBP, which is an important disadvantage of this method. Advantages of SIRT are the possibility to incorporate prior knowledge, the robustness with respect to noise, and the higher accuracy compa-

red to FBP for limited-data problems and projection angles that are not equiangularly distributed. The bottom row of Fig. 1.2 contains reconstructions of SIRT for varying parameters.

1.4 PREVIEW

Substantial research efforts have been made to improve the reconstruction accuracy of the computationally efficient FBP method. This can be done for example by various pre- and postprocessing steps, or by using different filters. We will focus in this work on the filtering step for two-dimensional reconstruction problems in X-ray computed tomography.

In Chapter 2 *'Fast Approximation of Algebraic Reconstruction Methods for Tomography'*, we introduce a new algorithm to create filters for FBP which are based on a linear algebraic reconstruction method. This method is called *Algebraic filter-Filtered Backprojection* (AF-FBP). The filters that are created can be used in FBP in the same way as for example the Ram-Lak filter. The image characteristics of the reconstructions of AF-FBP are similar to those of the linear Algebraic Reconstruction Method (ARM) that was used to create the filters. The main benefit of this method is that, once the filters have been created, reconstructions are created with the computational efficiency of FBP, while the favorable reconstruction accuracy of the linear ARM is largely preserved.

By design, the reconstruction of an ARM does not only depend on the projection data, but also on the size and shape of the reconstruction grid. Also the position of the object within the reconstruction grid has an effect on the reconstruction. Both these effects and the discretization effects in FBP are examined in Chapter 3 *'Spatial Variations in Reconstruction Methods for CT'*.

The method AF-FBP uses by design a single pixel of the reconstruction grid for the creation of the filters. In the experiments in Chapter 2, the central pixel of the reconstruction grid is chosen for reasons that are explained there. As a consequence of the results in Chapter 3, choosing a different pixel will lead to different filters. We have therefore investigated the idea to use several pixels in the reconstruction grid to create multiple filters which can be applied to smaller areas of the reconstruction grid. The implementation and results for applying

these *local* filters is presented in Chapter 4 *'Approximating Algebraic Tomography Methods by Filtered Backprojection: a Local Filter Approach'*.

The AF-FBP algorithm presented in Chapter 2 is applicable for linear ARMs. It is not applicable for nonlinear ARMs such as the Conjugate Gradient Least Squares (CGLS) method or the Expectation Maximization (EM) method. Since also these methods are computationally inefficient compared to FBP, we would like to be able to approximate these methods with a fast algorithm that is similar to AF-FBP. In Chapter 5 *'Algebraic Filter Approach for Fast Approximation of Nonlinear Tomographic Reconstruction Methods'*, the method AF-FBP is extended such that it can also be used for certain types of nonlinear algebraic reconstruction methods.

Computed tomography is used in various application fields, for example in industrial and (bio)medical imaging. In the experiments conducted in the previously announced chapters, the projection data were either simulated by computer models or obtained for industrial imaging applications. In biomedical imaging, bone structures and soft tissues with various gray levels are reconstructed. Especially for soft tissues, the difference in gray levels between neighboring tissues can be small and the boundaries can be highly irregular. In Chapter 6 *'Filtered Backprojection using Algebraic Filters; Application to Biomedical Micro-CT Data'*, we compare reconstruction results of AF-FBP and FBP with a selection of standard filters for two experimentally obtained projection data sets of small animals.

We conclude this thesis with a comparison of several recently proposed methods to create and apply filters for FBP. The algorithms in Chapter 7 *'The accuracy of FBP with recently introduced filters: a comparison'* can all be applied to two-dimensional parallel beam geometries. We provide a short description of these methods and give an overview of their characteristics including the computational efficiency. We also comment on the reconstruction quality based on experimental results.

BIBLIOGRAPHY

[1] S. Van Aert et al. Three-dimensional atomic imaging of crystalline nanoparticles. *Nature* 2011; 470(7334): 374–377.

[2] H. Sipila. Moving object computer-tomography for luggage inspection. *Applications of Signal and Image Processing in Explosives Detection Systems*. Ed. by M. C. Connelly and S. M. Cheung. Proc. SPIE, 1993; 1824: 39–40.

[3] P. Targowski et al. The Application of Optical Coherence Tomography to Non-Destructive Examination of Museum Objects. *Studies in Conservation* 2004; 49(2): 107–114.

[4] M. Defrise and G. T. Gullberg. Image reconstruction. *Phys. Med. Biol.* 2006; 51(13): 139–154.

[5] W. A. Kalender. X-ray computed tomography. *Phys. Med. Biol.* 2006; 51(13): 29–43.

[6] T. M. Buzug. *Computed Tomography: From Photon Statistics to Modern Cone-Beam CT*. Berlin: Springer, 2008.

[7] A. Markoe. *Analytic Tomography*. New York: Cambridge University Press, 2006.

[8] J. Radon. Über die Bestimmung von Funktionen durch ihre Integralwerte längs gewisser Mannigfaltigkeiten. *Berichte Sächsiche Akademie der Wissenschaften* 1917; 69: 262–277.

[9] F. Natterer. *Mathematical methods in image reconstruction*. Philadelphia: SIAM, 2001.

[10] A. C. Kak and M. Slaney. *Principles of Computerized Tomographic Imaging*. Philadelphia: SIAM, 2001.

[11] G. T. Herman and A. Kuba, eds. *Discrete Tomography: Foundations, Algorithms and Applications*. Birkhäuser, Boston, 1999.

[12] G. N. Ramachandran and A. V. Lakshminarayanan. Three-dimensional Reconstruction from Radiographs and Electron Micrographs: Application of Convolutions instead of Fourier Transforms. *Proc. Nat. Acad. Sci. USA* 1971; 68(9): 2236–2240.

[13] G. T. Herman. *Fundamentals of Computerized Tomography: Image Reconstruction from Projections*. Berlin: Springer, 2009.

[14] A. van der Sluis and H. A. van der Vorst. SIRT- and CG-type methods for the iterative solution of sparse linear least-squares problems. *Linear Algebra and its Applications* 1990; 130: 257–302.

[15] D. Castano-Diez, H. Mueller, and A. S. Frangakis. Implementation and performance evaluation of reconstruction algorithms on graphics processors. *Journal of Structural Biology* 2007; 157(1): 288–295.

[16] F. Xu and K. Mueller. Accelerating Popular Tomographic Reconstruction Algorithms On Commodity PC Graphics Hardware. *IEEE Trans. Nucl. Science* 2005; 52(3): 654–663.

[17] W. J. Palenstijn, K. J. Batenburg, and J. Sijbers. Performance improvements for iterative electron tomography reconstruction using graphics processing units (GPUs). *J. Struct. Biol.* 2011; 176(2): 250–253.